Optimal Design of K-space Trajectories Using a Multi-objective Genetic Algorithm

B. M. Dale[1], J. S. Lewin[1,2], J. L. Duerk[1,2]

[1]Case Western Reserve University, Cleveland, Ohio, United States, [2]University Hospitals of Cleveland, Cleveland, Ohio, United States

Introduction: Spiral, radial, and other non-rectilinear *k*-space trajectories are an area of active research in MRI due largely to their typically rapid acquisition times and benign artifact patterns. Trajectory design has commonly proceeded from description of a simple shape to investigation of its properties. Instead, it would be desirable to specify the desired properties of the acquisition, and then derive a trajectory that best achieves those objectives. Here a multi-objective genetic algorithm is used to design trajectories with beneficial time, aliasing, flow, and off-resonance properties.

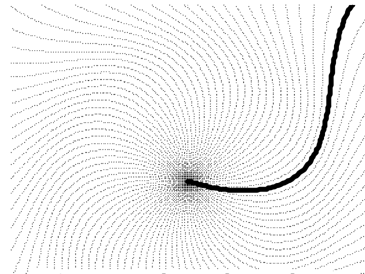

Fig 1. Example GA-designed trajectory. Has non-zero gradient amplitude at k-space origin.

Methods: Genetic algorithms (GA's) use a probabilistic biological metaphor rather than a deterministic hill-climbing metaphor [1]. Relative to traditional methods, GA's are more able to find global optima in the face of ill-behaved objective and constraint functions. In addition, multi-objective GA's sample the entire Pareto-optimal set in a single run.

Imaging and optimization objectives were chosen for their potential impact on image quality and not for linearity or other purely mathematical considerations. Artifact severity is the main image-quality property of a trajectory. Specifically, the four objectives considered here were acquisition time, aliasing energy, flow artifact energy, and off-resonance artifact energy. The acquisition time was calculated as: $N_{leafs} + t_{leaf}/100$, where N_{leafs} is the number of interleafs and t_{leaf} is the readout time in ms. Aliasing energy was calculated by evaluating a Lorentzian envelope at each unsampled point within a rectilinear grid: $E_A(k) = C_1/(C_2+|k|^2)$. Here, $|k|$ is the *k*-space radius and the constants are found by a least-squares fit to several actual spiral data sets. Measures of off-resonance and flow artifact energy used simulations with analytical phantoms [2]. Simulated data was generated and gridded onto a 2x over sampled matrix using the standard convolution-based gridding-reconstruction with Jackson's density compensation function for a width 1 rectangular convolution kernel [3]. This simulation was repeated during the optimization to generate three magnitude images for each trajectory, one without flow or off-resonance, one corrupted by flow, and one by off-resonance. Flow or off-resonance artifact was computed by the total energy of the difference between the uncorrupted and corrupted images.

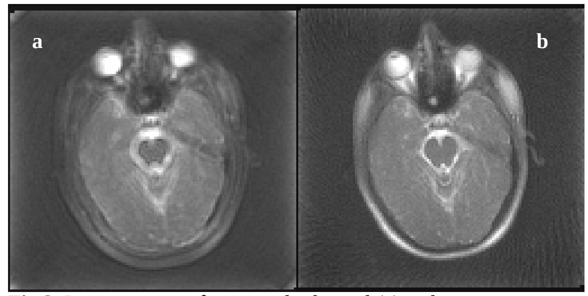

Fig 2. In-vivo images from standard spiral (a) and new trajectory (b). Note generally superior quality of (b).

The NSGA-II [4] was implemented in Mathematica 4.0 (Wolfram Research Inc., Champaign, IL). The population size was 200. Parent solutions were chosen through a binary tournament. Child solutions were obtained through simulated binary crossover (μ_c=3) between the parents followed by lognormal mutation (P_m=0.01, σ_m=0.5) on the child [1]. 40 children were produced for 400 generations, resulting in approximately 16,000 trajectories examined. The optimization used a slew-rate constraint of 200 T/m/s and a gradient amplitude constraint of 40 mT/m. Peripheral nerve stimulation constraints were evaluated with the SAFE model [5]. The constraints were enforced through constrained non-dominated sorting [4].

Images using 20 trajectories were acquired on a 1.5 T Siemens Sonata (Siemens Medical Solutions, Erlangen, Germany) under conditions that recreate, as much as possible, the simulated images, with the number of averages set between 5 and 17 to both control for and reduce noise levels. Image reconstruction was performed by a table-lookup method for gridding reconstruction [6], with the tables calculated based on the measured trajectory. Linear regression was used to evaluate the effectiveness of the simulated objectives as independent linear predictors of the measured objectives.

Results: The algorithm converged to a well-defined set with standard spirals on the rapid but low-quality end, WHIRL [7] trajectories in the middle, and a new class of trajectories on the high-quality end. The new trajectories all begin with non-zero gradient amplitude at the *k*-space origin and curve outward gently relative to standard spirals, an example is shown in Fig. 1. An image acquired with this GA-designed trajectory is compared to one acquired with a standard spiral in Fig. 2.

Fig. 3 displays the correlation between the simulated and experimental measurements for each objective. The simulated and actual time objectives were the most strongly correlated (R^2=0.981) while the off-resonance objective measures were the least (R^2=0.770). In all cases the slope of the regression was positive with 95% confidence.

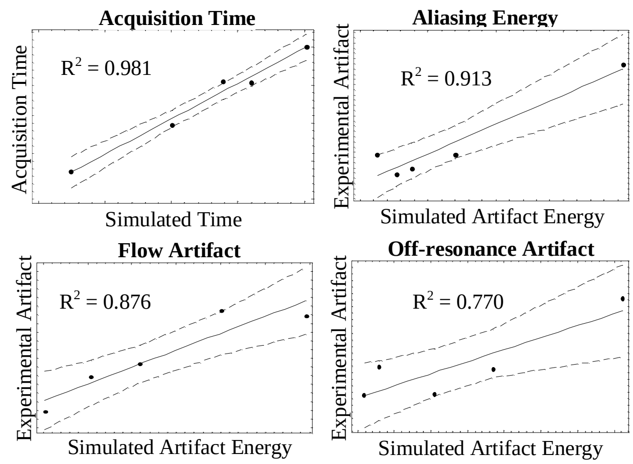

Fig. 3. Correlation between simulated objectives and experimental analogs. Solid line is regression, dashed are 90% confidence region.

Discussion: The waveforms and *k*-space trajectories resulting from the GA methodology have no specific analytic form with elements that are visually related to radial, spiral and WHIRL trajectories that form their genetic composition. Although the quality of the image (Fig. 2) acquired using the new trajectory is visibly superior to the image acquired with the spiral trajectory, it is incorrect to say that the new trajectory is superior to the spiral. Instead, the preferred trajectory's sacrifice in speed is worth the improvement in quality; clearly this depends on the requirements of a particular application.

The correlation between the simulated and experimental measures was positive with 95% confidence in all cases. Thus improvements in the simulated measures during the optimization generally resulted in measurably superior image quality. One factor that may have limited the strength of the correlation between the simulated and experimental objectives is that the various trajectories in each group are not exactly uniform in the other three objectives. Additionally, the baseline images for the off-resonance cost function, and all images for the aliasing and flow cost functions, are unavoidably corrupted by some amount of off-resonance.

The particular objectives chosen here impact the specific result of this optimization rather than the general applicability of the optimization technique. In this sense, the fact that the algorithm was able to converge to a well-defined set of non-dominated trajectories may prove to be more important than the derivation of the particular trajectory presented in Fig. 1. Specific applications may demand a different set of objectives, or even a different set of parameters, but the convergence, robustness, and other properties of the genetic algorithm itself will remain. As robust and effective design procedures are developed and utilized, the quality of future techniques can be more rapidly improved relative to the normal progress and the quality will be less dependent on the sequence-development skills of the designer. Such design procedures would be desirable in order to ensure that patients consistently receive the highest quality of care.

Conclusion: We have presented a technique for the optimal design of *k*-space trajectories. This technique allows the specification of the desired properties of the trajectory followed by a GA based search through all possible trajectories to find those that optimally accomplish the specified objectives. Reduction of the simulated artifact levels during the optimization was correlated with reduced artifact levels in the experimentally acquired images. We believe the method has significant potential for improving the utility and quality of non-rectilinear *k*-space trajectories. Novel trajectories with specific image-quality properties can now be derived without violating critical hardware or patient-safety constraints. We also believe that extensions to this method will have similar potential for improving most MR image acquisition techniques.

References: [1] Deb. Mult.-obj. opt. evol. algo. 2001. [2] Nishimura. MRM 33: 549-56. 1995. [3] O'Sullivan. IEEE TMI. MI-4: 200-7. 1985. [4] Deb. IEEE T. Evol. Comp. 6: 182-97. 2002. [5] Hebrank. Proc. ISMRM. 1310. 2000. [6] Dale. IEEE TMI. 20: 207-17. 2001. [7] Pipe. MRM. 42: 714-20 1999.